Hindawi
Modelling and Simulation in Engineering
Volume 2022, Article ID 8209487, 12 pages
https://doi.org/10.1155/2022/8209487

Research Article

A Study on Wind Pressure Characteristics of a Large-Span Membrane Structure under the Fluctuating Wind in a Vertical Direction Based on a Large Eddy Simulation

Fangjin Sun,[1,2,3] **Haoxuan Tang**,[3] **Mingjin Lu**,[4] **Daming Zhang**,[3,5] **and Chen Lu**[3]

[1]*Guangxi Key Laboratory of New Energy and Building Energy Saving, Guilin 541004, China*
[2]*Guangxi Key Laboratory of Geomechanics and Geotechnical Engineering, Guilin 541004, China*
[3]*College of Civil Engineering and Architecture, Guilin University of Technology, Guilin 541004, China*
[4]*College of Civil Engineering, Liaoning Technical University, Fuxin 123000, China*
[5]*Guangxi Key Laboratory of Embedded Technology and Intelligence, Guilin 541006, China*

Correspondence should be addressed to Daming Zhang; e_horse@163.com

Received 26 March 2022; Revised 10 October 2022; Accepted 11 October 2022; Published 14 November 2022

Academic Editor: Houari Ameur

This paper reports the wind pressure characteristics on long-span roofs under fluctuating wind in a vertical direction based on a large eddy simulation (LES). Three types of roofs, i.e., saddle, wavy, and continuous arch roofs, are tested. First, the membrane structure canopy is measured, and the model is established for numerical simulation. The computational models and methods are verified by comparing the obtained wind pressure distributions on the roof with the measured results and numerical simulation results under other methods. Next, a numerical simulation is performed to understand not only the wind pressure and the wind speed time series but also the wind vibration responses and fluid-solid coupling. The effects of lateral fluctuating wind at different wind speeds on the wind-induced vibration response and wind pressure distribution of different membrane structures are studied. Based on the results, the wind pressure zones of the roofs are discussed. Furthermore, the original structures are optimized and numerically simulated considering the streamlined design concept to study the influence mechanism of fluctuating wind on the roof in more detail.

1. Introduction

Membrane structure has low mass, low stiffness, large flexibility, and long natural vibration period, which determines that membrane structure is a kind of wind-sensitive building structure. To reduce the influence of wind on the structure surface, it is very important to study the response of wind pressure and wind-induced dynamic responses. A wind tunnel experiment is an effective method, which can directly obtain model experimental data, but it is expensive and experimental data are limited [1]. Therefore, from an economic point of view, the combination of finite element (FE) analysis and computational fluid dynamics (CFD) simulation is a more cost-effective and attractive method to gain a deeper understanding of the interaction between the two processes.

FE is widely used in structural calculation and has been proven to be a reliable and effective method. Many kinds of literature have studied complex structural problems. For example, Zhu et al. [2] analyzed the fatigue reliability of full-size blades based on the probability S-N curve and stochastic finite element simulation combined with sampling technology. Chen et al. [3] analyzed in detail the progressive failure behavior of the trailing edge part of the wind turbine blade and established a nonlinear finite element model on this basis. Evangelos et al. [4] take offshore wind turbines (OWT) as the research object and use 3D finite element (FE) modeling to analyze the dynamics of the OWT-monopile-soil system.

Part of the simulation is based on Reynolds-averaged Navier–Stokes equations (RANS) to simulate the turbulence that occurs, such as [5, 6]. RANS requires fewer computing

resources and can quickly calculate and solve turbulence. Because RANS decomposes the instantaneous part of the N-S equation into the average part and the pulsation part, and only calculates the average part, the calculation accuracy of RANS is poor, and the calculation results are partially inconsistent with the real situation [7]. But even so, RANS is still widely used in the world.

Some studies [8] show that large eddy simulation (LES) has higher superiority than the RANS model. The simulation based on LES can describe the turbulence motion more accurately because the calculation of LES is based on the locally isotropic hypothesis [9], which classifies turbulence in terms of structure scale. The large scale is anisotropic, the small scale is isotropic, and RANS is to average the whole structure. Although LES is more accurate, it is significantly more computationally intensive than RANS. Simulation based on LES has studied many problems, from the influence of the location of the windward inlet on the ventilation volume and flow field inside the building [10], to the accurate prediction of outdoor microclimate and thermal comfort conditions in urban planning [11]. As well as the aerodynamic response of standard high-rise buildings [12], factors influencing the flow and dispersion simulation around an isolated building [13] and many others.

Membrane-structure building is a special building in modern times, and its wind effect is concerned by many documents. Nagai et al. [14] took the unit horn-shaped membrane roof as the research object, carried out the wind tunnel test under turbulence, and obtained its representative wind pressure. Yue et al. [15] measured and analyzed the response and wind speed of two saddle-shaped tensile membrane structures under uniform flow. Arjun et al. [16] studied the influence of arch span ratio, arch span, and other factors on the wind resistance of membrane structures through wind tunnel tests on closed and open models. Despite these works, there is still a lack of research on the effect of vertical wind on the surface of membrane structures in the literature. The membrane structure is greatly affected by the vertical wind, while the vertical wind effect of high-rise buildings can be ignored [17, 18]. This phenomenon is largely due to the strong wind vibration response. The wind-induced vibration response caused by the horizontal wind is nearly vertical to the horizontal plane [19], which can be superposed with the wind-induced vibration response caused by the vertical wind to amplify its effect. Sun et al. [20] found that the displacement after the vertical wind participation increased by 1.57-2.94 times compared with the horizontal wind alone. Therefore, LES is used to study the effect of vertical wind on membrane structure.

The second section gives the correctness and feasibility of LES-based simulation. The third section describes the model establishment and program setting. The fourth section gives the simulation results. The fifth section summarizes the wind pressure coefficient zoning based on the obtained results. The sixth section gives the optimization model and the analysis process. The seventh section is the conclusion.

2. Verification of the Method

In the present study, the reliability and accuracy of the LES can be verified by comparing the measurements with results from multiple turbulence models.

2.1. Wind Pressure Measurement. The measured object is a membrane canopy located on the campus of the Zhejiang University of Technology. The height of the membrane canopy is about 4.5 m. The total measurement span and the length of the wind pressure sensor line are 4 m and 10 m, respectively. The wind pressure sensor of the measuring equipment is a CY2000F wind pressure transmitter, and the measuring range of the instrument is -1.5 ~ 1.5 kpa. The equipment of the wind pressure acquisition system is placed horizontally on the ground to ensure the effectiveness of wind pressure measurement. It is impossible to place more wind pressure sensors on its surface due to the lightweight and large flexibility of the membrane canopy. Too many sensors will seriously affect the measurement results. To obtain an accurate wind pressure value and reduce the influence of the sensor on the airflow, the measuring point is arranged at the edge of the canopy membrane structure. The vibration at this place is small, which can not only reduce the interaction between them but also measure the effective pressure value.

2.2. Settings. An ICEM is used to build the calculation model. The canopy model is 32 m long and 4 m wide. The lowest and highest position of the canopy model is 1.9 m and 3.9 m away from the ground, respectively. The computational domain model sizes are set to 180 m × 120 m × 60 m, corresponding to the x, y, and z axes in the coordinate axis, respectively. The placement position of the model is 1/3 long edge away from the entrance of the calculation domain. The structure of the calculation model is divided into tetrahedral meshes, and the meshes of the surrounding area and the model are encrypted.

Enter the boundary condition panel, the boundary condition at the outlet is free outflow, and the wall condition is nonslip boundary condition. Solution panel selects simple pressure correction mode, the upwind discrete scheme with second-order accuracy is selected for the diffusion term, select residual convergence in the monitor's panel, and set the convergence accuracy to 0.0001.

2.3. Results. Figure 1 shows that the simulation results are close to the measured results. The variation law at each measuring point is similar. The accuracy of the LES can be proved by comparing different results.

3. Analysis of Wind Speed Time Series

In this section, the wind speed time series of different roofs is analyzed by large eddy simulation and MATLAB AR method. The detailed analysis process is as follows.

3.1. Characteristics of Fluctuating Wind. The three main characteristics of fluctuating wind are the power spectrum of fluctuation wind speed, turbulence integral scale, and

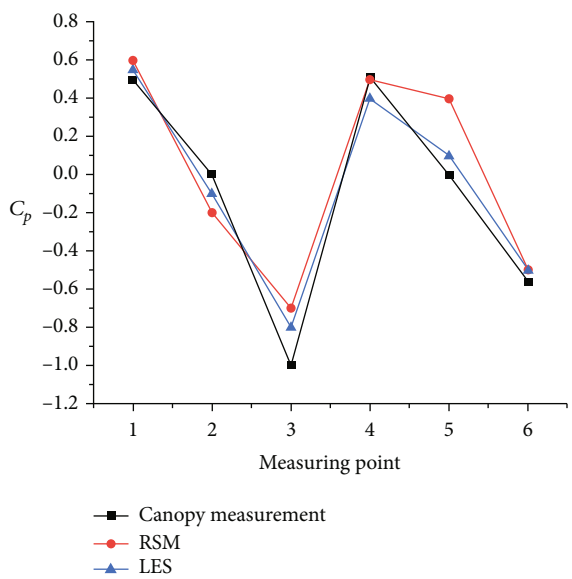

Figure 1: Comparison diagram of wind pressure coefficient. C_p is the wind pressure coefficient. Different points are analyzed by different methods (square for canopy measurement; circle for RSM; triangle for LES).

Table 1: Dimensions of the calculation model.

Model	Structural depth H (m)	Structure length L_2 (m)	Structure width L_1 (m)
Arch	0.2	2.0	0.8
Saddle	0.2	0.8	0.8
Wavy	0.2	2.0	0.8

turbulence intensity [21]. In short, the pulsating wind comes from the irregular flow of the wind, and its intensity changes randomly with time. Fluctuating wind can be regarded as a random variable, which is usually described and explained by using mathematical statistics.

Turbulence intensity is a parameter used to describe atmospheric turbulence. Its value is not related to the long and short periodic changes of wind. The mathematical definition of turbulence intensity may be represented by the following equations:

$$I(z) = \frac{\sigma_{\mathrm{vf}}(z)}{\bar{v}(z)}, \tag{1}$$

where $\bar{v}(z)$ is the average wind speed and $\sigma_{\mathrm{vf}}(z)$ is the root mean square value of wind speed.

The turbulence integral scale is an integral function whose variable is the turbulence correlation coefficient, which can be measured in time or space. It plays a decisive role in the size of vortices in the space flow field. The formula of turbulence integral scale may be represented by the following equations:

$$L = \frac{1}{\sigma_u{}^2} \int_0^{\infty} R_{u1u2}(r)\mathrm{d}r, \tag{2}$$

where $R_{u1u2}(r)$ is the cross-covariance function formula of u_1 and u_2 and $R_{u1u2}(r)$ is the value of root mean square of u_1 and u_2.

3.2. Method of Generating Fluctuating Wind. There are three methods for the artificial generation of fluctuating wind present: harmonic superposition method, wavelet transform method, and linear filter method. A linear filter method is divided into the autoregressive moving average algorithm model and the AR model. In this chapter, an AR algorithm, also known as an autoregressive algorithm model, is applied to simulate the vertical fluctuating wind load on the surface of roofs.

The autoregressive algorithm model is to describe the relationship between a group of random sequences at time t and the regular changes of the previous p time sequences in the past, and also describes the relationship between random sequences and white noise at time t.

The autoregressive algorithm model may be represented by the following equations:

$$z_t = \sum_{i=1}^{p} \varphi_i z_{t-i} + \varepsilon_t, \tag{3}$$

where t is the time value, p is the order value of the AR model, φ_i is the model parameter value, and ε_t is the white noise at time t.

Due to the spatiality of the fluctuating wind, the magnitude and direction of wind speed at various positions on the structural surface may not occur synchronously or even irrelevantly. Therefore, it is necessary to convert this random process into N correlated random processes by mathematical transformation.

The random processes can be obtained from the following equations:

$$\begin{aligned} V_j(t) &= \sum_{i=1}^{N} C_{\mathrm{jj}} \cdot V_{\mathrm{oi}}(t), \\ C_{\mathrm{jj}} &= \sqrt{\left(\frac{R_{\mathrm{ji}}}{\sigma_n^2}\right) - \sum_{k=1}^{j=1} C_{\mathrm{jk}}^2}, \\ R_{\mathrm{ji}} &= \int_0^{\infty} S_v\left(p_i, p_j, n\right)\mathrm{dn}, \end{aligned} \tag{4}$$

where C_{jj} is the matrix value, $V_{\mathrm{oi}}(t)$ is the wind velocity, t is the time, and $S_v(p_i, p_j, n)$ is a random function.

It is necessary to select the three-dimensional spatial coherence function for different shapes of roofs in the present study, and it can be represented by the following equation:

$$\gamma\left(p_i, p_j, n\right) = \exp\left(-\frac{2n\left[C_x^2\left(x_i - x_j\right)^2 + C_y^2\left(y_i - y_j\right)^2 + C_z^2\left(z_i - z_j\right)^2\right]^{1/2}}{V_{pi} + V_{pj}}\right). \tag{5}$$

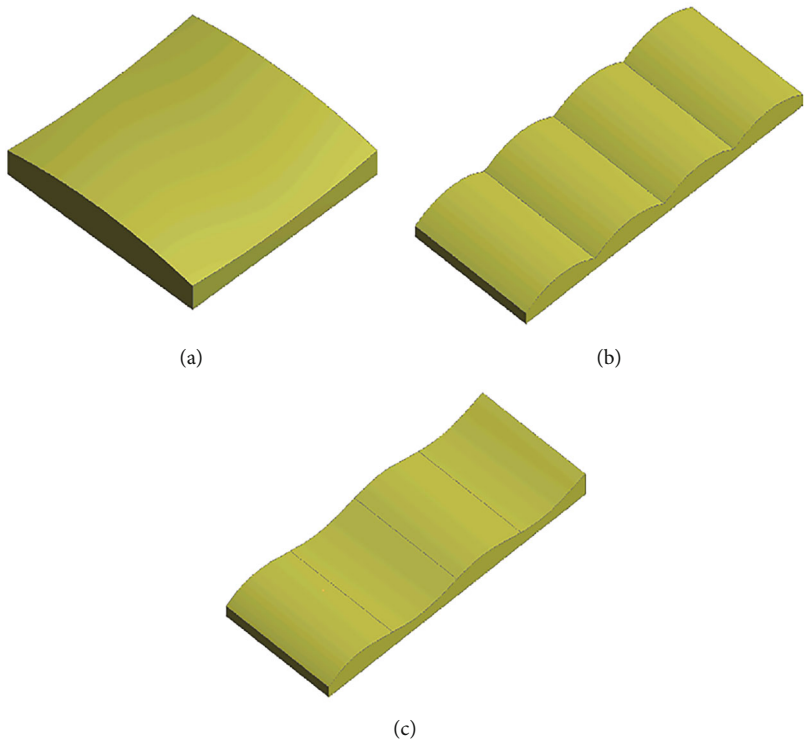

Figure 2: Three different forms of membrane structure models. (a) Saddle-shaped roof, (b) continuous arch roof, and (c) wave-shaped roof. The specific dimensions are shown in Table 1.

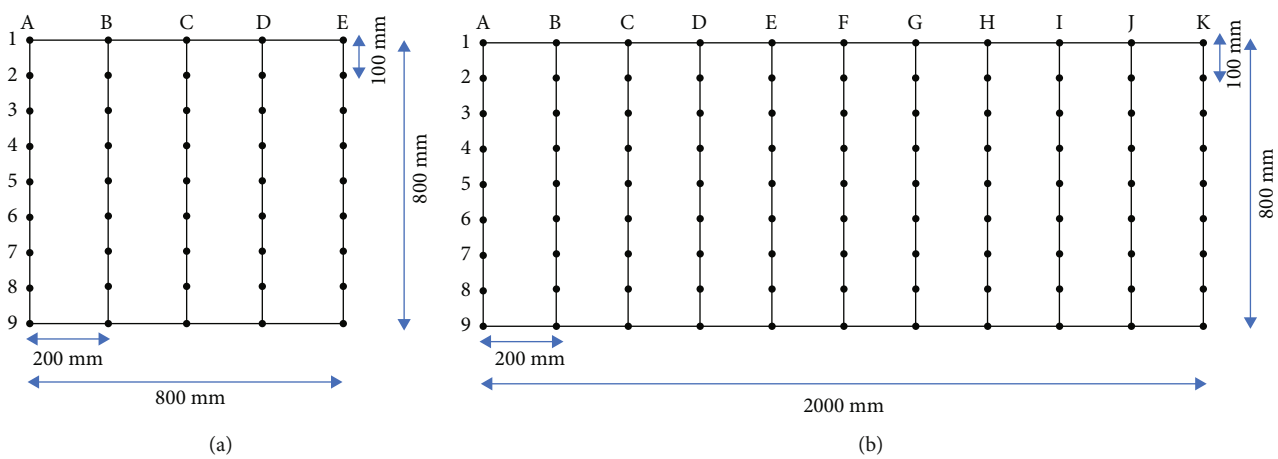

Figure 3: (a) Saddle roof measuring points. (b) Arched and wavy roof measuring points. The spacing between measuring points is uniform.

The C_x, C_y, and C_z are spatial attenuation coefficients in the equation.

3.3. Settings and Results. Three roof shapes, i.e., saddle, wavy, and continuous arch roofs, are used in this study. The models are built in UG and imported into the ICEM plate of ANSYS WORKBENCH 19.0 for meshing. The size scaling ratio of 1 : 100 is adopted in the model. Table 1 shows the three model sizes. Figure 2 shows three membrane structure models.

Loading the numerical simulation program into the computational simulation software. The commonly used Davenport wind spectrum for fluctuating wind speed spectrum selection. The C_x, C_y, and C_z are selected as 16 m, 8 m, and 10 m, respectively. The ground roughness coefficient K in the wind spectrum is 0.0046, the order p is 4. The time step is 0.1 s, and the duration is 100 s.

The program is based on the mentioned use of MATLAB through the AR method. The Davenport wind spectrum is essentially a fluctuating wind spectrum at a height of 10 m.

The uniform arrangement of measuring points is applied to the membrane structures of different shapes. Figure 3(a) shows the distribution diagram of saddle measuring points. Figure 3(b) shows the diagram of the distribution of arched

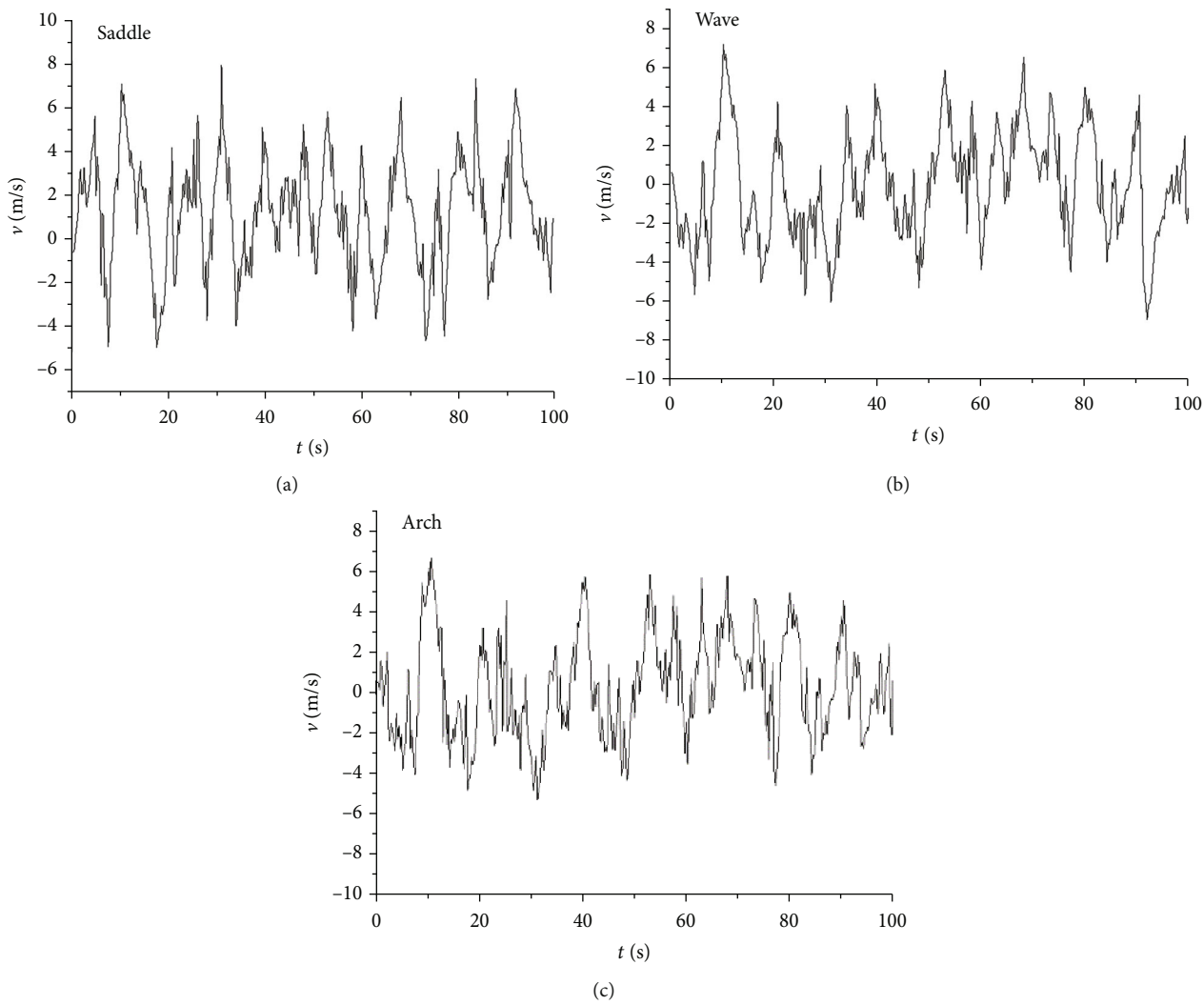

Figure 4: (a) Wind speed time series of the saddle roof. (b) Wind speed time series of the wave-shaped roof. (c) Wind speed time series of the continuous arch roof. v is the fluctuating wind speed; t is the time series. The fluctuating wind acts on the roof surface vertically.

and wavy measuring points. Figure 4 shows the time-series data of vertical fluctuating wind speed for the three roof surfaces, the data obtained from the simulation of the spatial wind field.

4. Wind-Induced Response of the Long-Span Membrane Structures under Vertical Wind

The wind pressure distribution can be obtained from a simulation analysis of various shapes by a mathematical formula of wind pressure-wind speed conversion. Then, the relationship between the fluctuating wind velocity spectrum and pressure spectrum on the roof surface needs to be established because of the size and direction of the fluctuating wind at different locations due to uneven roof height.

4.1. Results of Saddle Roof. Figure 5 shows the results of the wind-induced response of the saddle roof under a vertical fluctuating wind load.

It can be found that the vibration response frequency is not uniform to the response diagram shown in Figure 5, but the frequency shows a trend of strengthening with time in the calculation period. The amplitude of wind vibration response increases with the increase of wind speed, but the general trend is consistent with Figures 5(a)–5(c) diagram comparison. The curve vibration is extremely violent, and there are many peaks and valleys in the latter half of the time. It shows that the effect of fluid-solid coupling is directly related to the effect of wind vibration caused by the vertical fluctuating wind load. The violent vibration of the curve illustrates the randomness and irregularity of the vertical fluctuating wind load, the incoming flow is no longer a laminar flow, but an irregular flow. The obvious burr phenomenon in the velocity time series indicates that the saddle roof is greatly affected by the vertical fluctuating wind. The effect of vertical fluctuating wind load on wind-induced vibration response of the saddle roof is obvious. This situation should be considered in wind-resistant design and engineering research of saddle membrane structure.

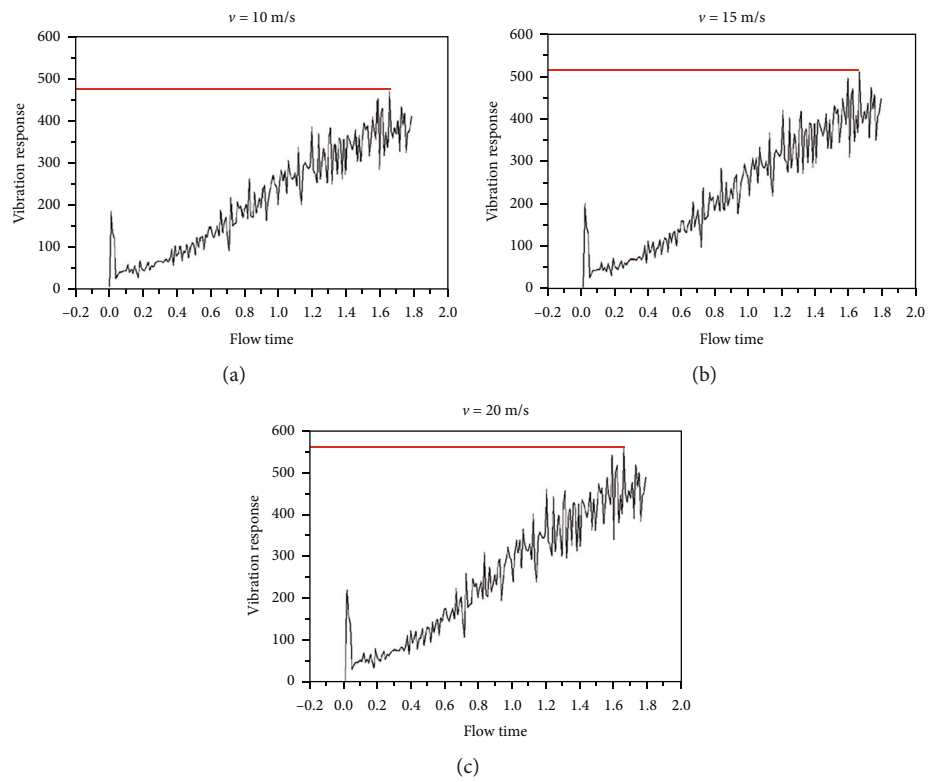

Figure 5: Wind-induced vibration responses of the saddle roof at different wind speeds, $v = 10$ m/s (a), $v = 15$ m/s (b), and $v = 20$ m/s (c). The red line indicates the maximum vibration response value.

4.2. Results of the Wave-Shaped Roof. Figure 6 shows the wind-induced response of a wave-shaped roof.

The initial wind vibration frequency is close to the tail wind vibration frequency shown in Figure 6, but the wind vibration response frequency is violent in the middle part of the time and there are more burrs. This phenomenon is attributed to the free frequency of the structure decreasing as the height of the wave roof surface changes. The response is also enhanced with the increase of fluctuating wind speed. The curve vibration amplitude of the surface increases and its vibration effect is very strong when the speed increases to 20 m/s. This phenomenon proves the remarkable effect of fluctuating vertical wind on the wave roof; it should be considered an important factor in the wind resistance design of large span membrane structures.

4.3. Results of the Arch Roof. Figure 7 shows the frequency of response on the continuous arch roof surface indicating a strengthening trend rather than a uniform state during the calculation period. With the increase in wind speed, the amplitude of vibration response also increases from the comparison of Figures 7(a)–7(c), but the general trend is consistent. Curve vibration is violent and there are many peaks and valleys when the speed reaches 20 m/s.

The results indicate that the interaction between fluid and solid is directly related to the effect of vertical fluctuating wind vibration. On the other hand, this vibration is random and irregular, and the incoming flow is also irregular. Furthermore, the membrane structure is clearly affected by the wind load. The influence is positively correlated with wind speed. The obvious burr phenomenon in the velocity time series indicates that the continuous arch roof is greatly affected by the vertical fluctuating wind.

4.4. Partition of Fluctuating Wind Pressure Coefficient on the Roof Surface. The wind pressure coefficient data are obtained from the simulation as mentioned and the arrangement of measuring points. The values of the pressure coefficient partition of different roofs under different wind speeds are given in the present study. The value shown in Figure 8 is obtained by considering the influence of different wind speeds on the wind pressure distribution and selecting the pulsating wind at a vertical angle.

5. Structure Optimization of Saddle and Arch Membrane

The main characteristics of streamlined objects are small resistance and high speed and so on. The value of air resistance on a windward surface of the streamlined object is the smallest, but an object with an irregular shape is affected by various air resistances of different sizes. The streamlined design can minimize the influence of air resistance on the surface of the membrane structure, reduce the flow separation of incoming flow on the surface of the material, decrease the structural damage, and improve the service life.

In this section, the influence of aerodynamic factors on the shape of the membrane structure is analyzed from

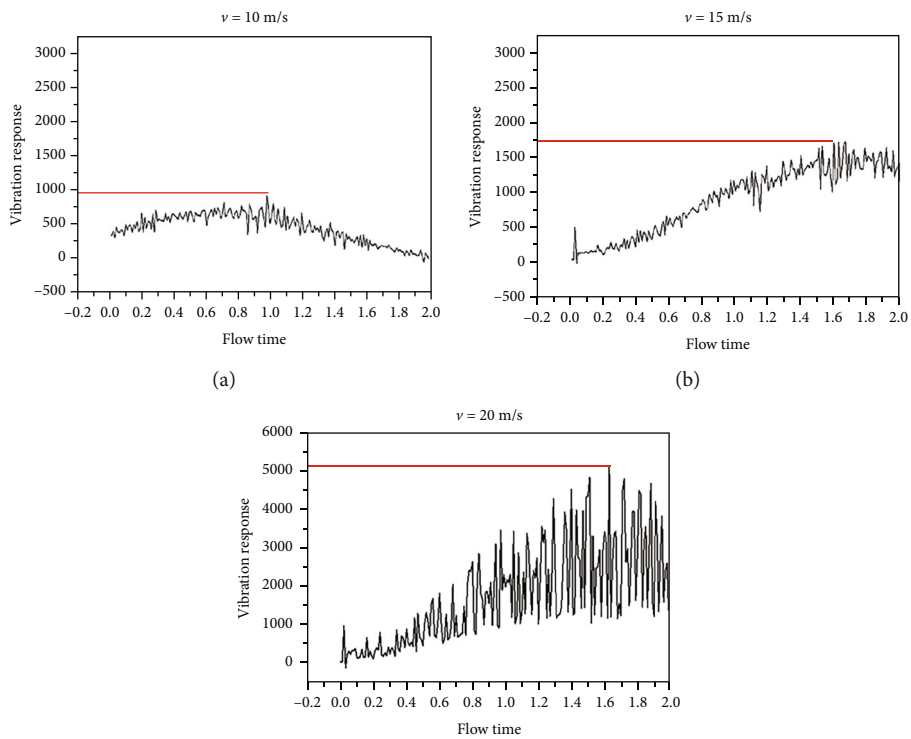

Figure 6: Wind-induced vibration responses of the wave-shaped roof at different wind speeds, $v = 10$ m/s (a), $v = 15$ m/s (b), and $v = 20$ m/s (c). The red line indicates the maximum vibration response value.

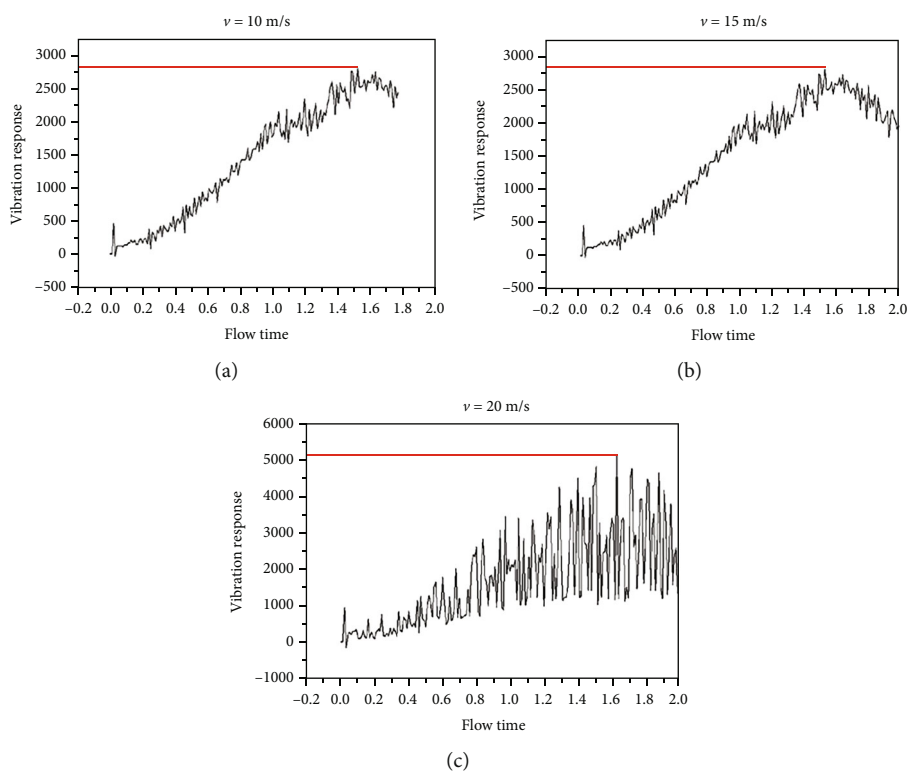

Figure 7: Wind-induced vibration responses of the arch roof at different wind speeds, $v = 10$ m/s (a), $v = 15$ m/s (b), and $v = 20$ m/s (c). The red line indicates the maximum vibration response value.

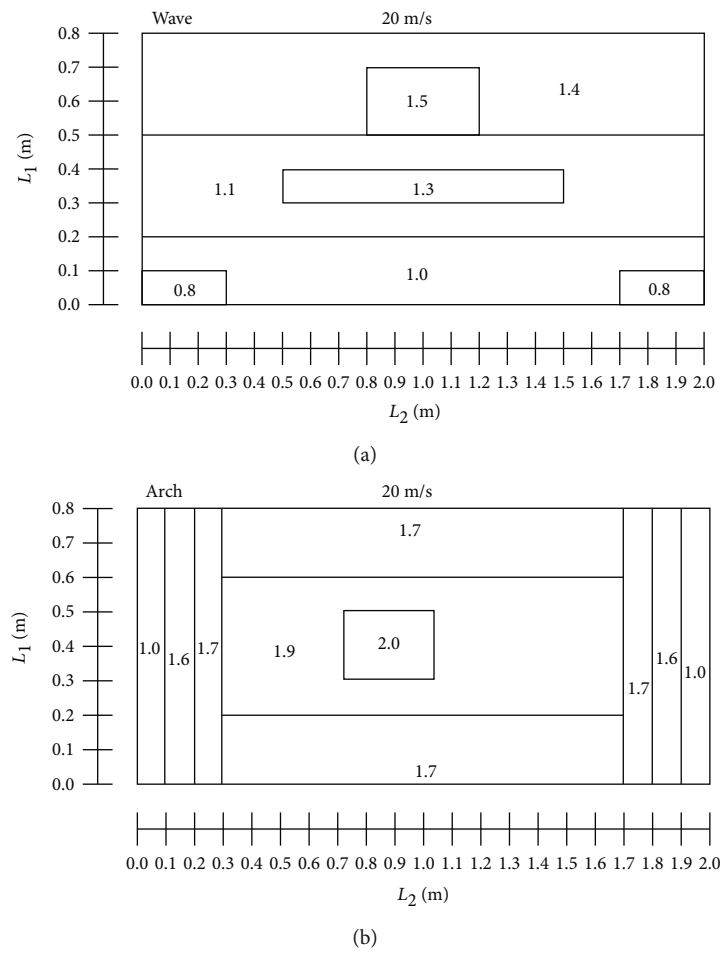

Figure 8: Partition diagrams of the wind pressure coefficients of the wave and arch roof at the same wind speed, $v = 20$ m/s (a, b). L_1 is the width of the model and L_2 is the length of the model, the unit is m.

multiple perspectives. It is found that the shape of roofs directly affects the air resistance on their surface. The function of streamlining design is realized by combining the requirements and ideas of streamlined design.

The original models (saddle and arch) are used as a basic model for a simulation, and its anti-interference ability to wind is analyzed according to the cloud chart of cross-sectional streamline change on its surface. Then, the shape of the surface of the basic model is fine-tuned to make the interface linearity more streamlined and improve its wind resistance.

5.1. Saddle Roof

5.1.1. Parameter Settings. The optimized model is a square enclosed saddle membrane structure with a quadrate frontal plane. The optimized model size is the same as the original model, as shown in Table 1. The size of the computational domain is $10\,\text{m} \times 16\,\text{m} \times 4\,\text{m}$, corresponding to the x, y, and z axes, respectively. The placement position of the model is 1/3 long edge away from the entrance of the calculation domain. An LES is applied to the simulation analysis of the optimized models. The total number of meshes is approximately 4,500,000.

5.1.2. Results and Discussion. Figure 9(a) shows the wind pressure distribution. It can be found that the pressure coefficient in the upper part is larger than the lower part and the pressure coefficient in the middle part shows a downward trend compared with the surrounding part. The maximum pressure coefficient is 93, the maximum value decreases by 713% compared to the unoptimized structure (757). The result shows that the optimization effect is obvious. The wind resistance of the membrane structure decreases, and the surface flow separation phenomenon is greatly improved, but the overall pressure coefficient distribution trend is not much different.

Figure 9(b) shows the displacement change. It can be found that the maximum deformation area is the concave area in the middle of the membrane structure and gradually decreases along both sides when the optimized structure is affected by a transverse wind. Therefore, the support should be strengthened in the concave area of a saddle membrane structure to improve its strength. The surface force deformation is also more uniform and there is no mutation phenomenon after the aerodynamic optimization of the structure.

Figure 9(c) shows the wind-induced response. The fluctuation range of the response value is 0-75, and the overall fluctuation range is small in the calculation period. There

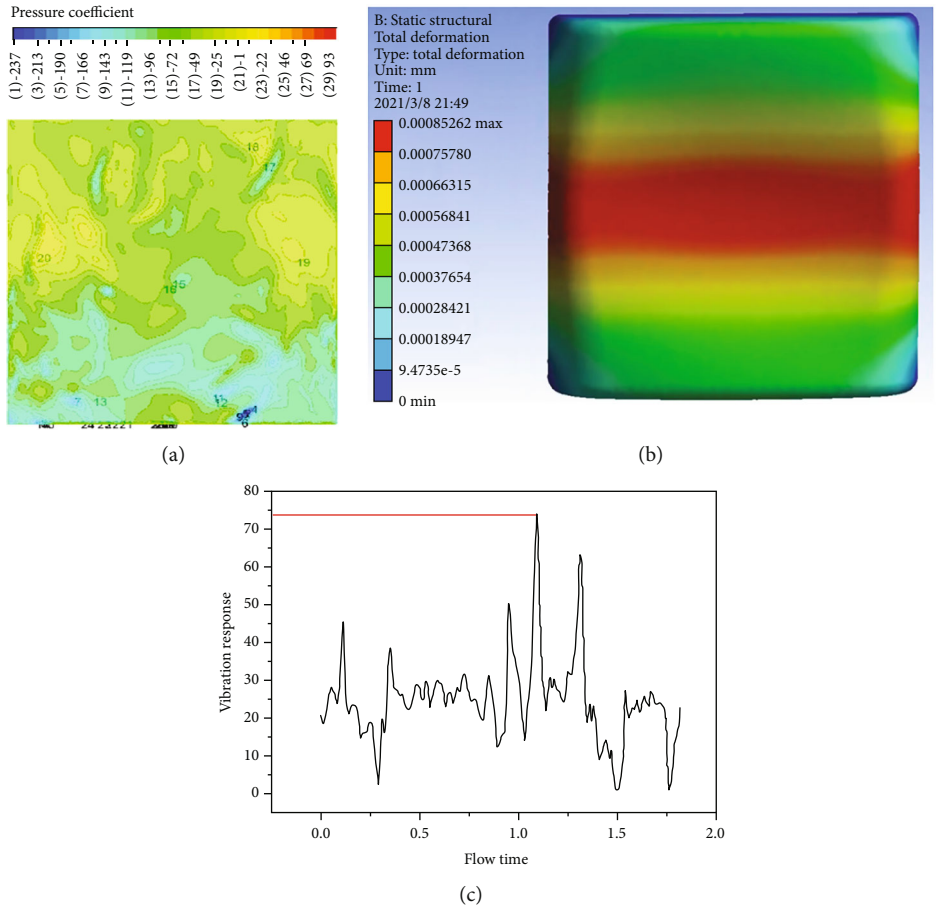

Figure 9: (a) Wind pressure distribution, blue indicates the minimum value and red indicates the maximum value. The gradient of color indicates different pressures. (b) Displacement diagram, the unit is mm. (c) Wind-induced response diagram, the red line indicates the maximum vibration response value.

are many peaks and valleys. The range of the wind-induced vibration response before the optimization is 0-450, the maximum value increases by 500% compared with the optimized results. It can be found that the perturbation effect of small flow on the roof surface decreases significantly after optimization. The decrease of the disturbance is beneficial to increasing structure life and reducing wind noise.

The stress, deformation, and wind pressure distribution of the optimized roof surface have been greatly improved. The improvement is mainly reflected in the decrease in wind resistance and maximum wind pressure, and the more uniform wind pressure distribution. However, the existence of the central depression area of the roof will form a local vortex pressure area after the airflow due to the structural form of the structure.

5.2. Arch Roof

5.2.1. Parameter Settings. The optimized model is a square enclosed saddle membrane structure with a quadrate frontal plane. The size of the optimized model is 0.8 m × 0.8 m × 0.3 m. The size of the computational domain is 10 m × 16 m × 4 m, corresponding to the x, y, and z axes, respectively. The placement position of the model is 1/3 long edge away from the entrance of the calculation domain. An LES is applied to the numerical simulation analysis of the optimized model. The total number of meshes is approximately 4,700,000.

5.2.2. Results and Discussion. Figure 10(a) shows the wind pressure distribution. The wind pressure distribution of the optimized structure shows a symmetrical trend along the flow direction. The maximum wind pressure is 183, which is lower than the unoptimized structures. The area with a large wind pressure coefficient is at the upper and lower arcs. The wind pressure coefficient decreases sharply near the middle, but it shows a small increase trend in the middle. The upper and lower sides of the central position of the inflow direction produce an elliptical vortex pressure region. The elliptical vortex region decreases gradually along the inflow direction but reaches the maximum wind pressure at the middle right position.

Figure 10(b) shows the displacement change. The deformation area of the arched model is only concentrated in the most protruding positions in the middle of the roof and shows a gradient downward trend along the circumference. There is no sudden change area in the middle. This phenomenon is due to the maximum air pressure on the central region of the top of the optimized structure. The maximum deformation of the structure is acceptable and does not

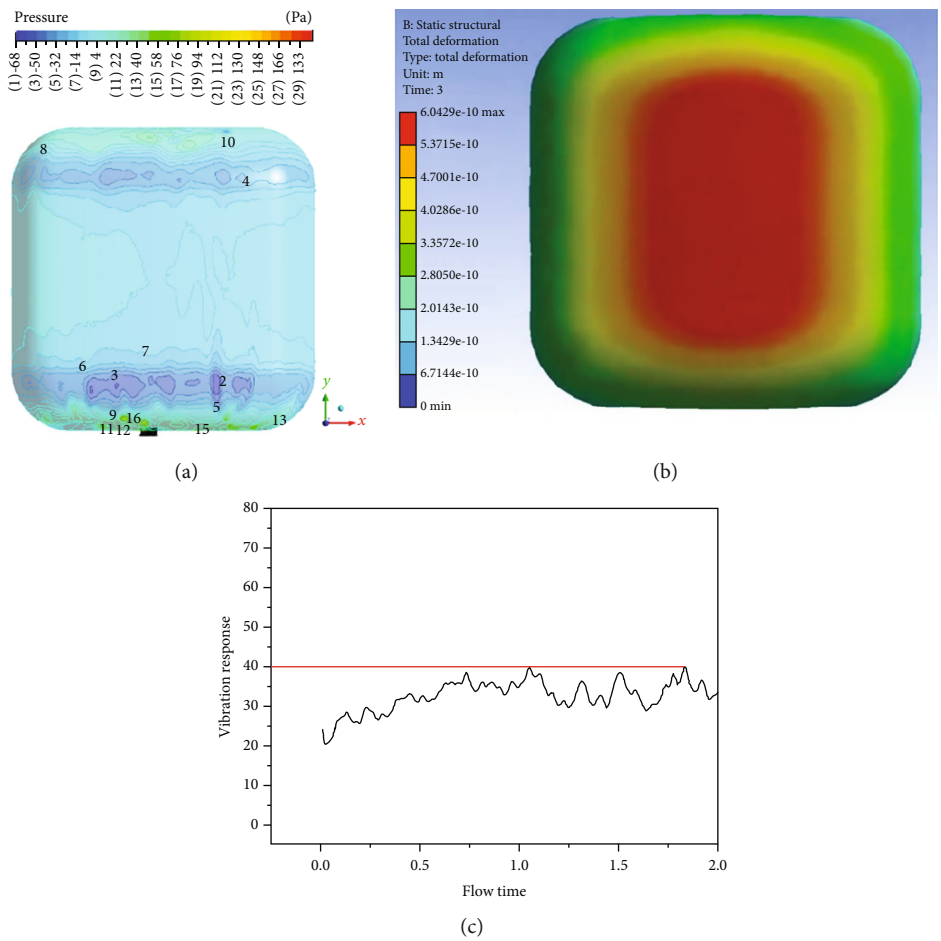

Figure 10: (a) Wind pressure distribution, blue indicates the minimum value and red indicates the maximum value. The gradient of color indicates different pressures. (b) Displacement diagram, the unit is m. (c) Wind-induced response diagram, the red line indicates the maximum vibration response value.

cause serious damage to the membrane structure and shorten the life cycle.

Figure 10(c) shows the wind-induced response of the arched model decreases clearly after optimization. The fluctuation range of wind-induced response is between 20 and 40, two orders of magnitude lower than the unoptimized structures. The surface flow of the structure is stable and there is no serious separation phenomenon.

The optimized arch membrane structure has good aerodynamic performance, uniform stress distribution, and good mechanical performance. The wind-induced vibration response has an obvious downward trend compared with that before optimization, and the wind-induced vibration response is good. The airflow on the surface of the membrane structure is very stable and there will be no wake separation.

6. Conclusions

Wind pressure and wind vibration response of three types of long-span roofs were investigated using a CFD simulation. First, the wind pressures on the canopy were computed to validate the LES turbulence model by comparing the results with the measured data. Next, the wind vibration response and wind speed time series can be obtained through simulation and measuring points, respectively. The wind vibration response results indicated that the effect of fluid-structure interaction is directly related to the wind-induced vibration response. The vertical fluctuating wind load has a significant effect on the wind-induced vibration response of the different roof surfaces. On the other hand, the three roofs are greatly affected by the vertical fluctuating wind. The wind-induced vibration response under vertical wind is in the same order of magnitude as that under the horizontal wind. Then, through the comparison of wind pressure data, the recommended value of wind pressure zoning under fluctuating wind load is given. Finally, to systematically understand the effect of vertical fluctuating wind on the roof, the streamlined design concept is applied to membrane structure optimization. The results indicated that the aerodynamic performance of the model structure has been significantly improved. In a future study, we will investigate the effects of wind vibration response and wind pressure on the roof in more detail.

Abbreviations

Nomenclature

LES: Large eddy simulation

Symbols

$\bar{v}(z)$:	Average wind speed
$\sigma_{\mathrm{vf}}(z)$:	Root mean square value of wind speed
$R_{u1u2}(r)$:	Cross covariance function formula of u_1 andu_2
$R_{u1u2}(r)$:	Value of root mean square of u_1 and u_2
t:	Time value
p:	Order value of the AR model
φ_i:	Model parameter values
ε_t:	White noise at time t
C_{jj}:	Matrix values
$V_{\mathrm{oi}}(t)$:	Wind velocity
$S_v(p_i, p_j, n)$:	Random function
C_x, C_y, C_z:	Space attenuation coefficients in the equation.

Data Availability

The data used to support the findings of this study are included within the article.

Conflicts of Interest

The authors declare that there are no conflicts of interest regarding the publication of this paper.

Acknowledgments

This study was supported by the National Natural Science Foundation of China (no. 52178468), Guangxi Key Laboratory of New Energy and Building Energy Saving Foundation (no. GuiKeneng 19-J-2114), Open Foundation of Guangxi Key Laboratory of Embedded Technology and Intelligence System (no. 2019-02-08), Joint Cultivation Program of National Natural Science Foundation of Guangxi (no. 2019GXNSFAA245037), Guangxi Youth Innovative Talents Research Project (no. Guike AD19245012), Guangxi Key Laboratory of Geomechanics and Geotechnical Engineering (no. GUIKENENG 19-Y-21-2), and the Scientific and Technology Startup Foundation of Guilin University of Technology (nos. GUTQGJJ2019042 and GUTQDJJ2019041).

References

[1] L. L. Zhang and C. T. Xie, "The experimental investigation of a high-rise building aeroelastic model," *Pneumatic experiment and measurement control*, vol. 2, pp. 19–24, 1991.

[2] S.-P. Zhu, Q. Liu, W. Peng, and X.-C. Zhang, "Computational-experimental approaches for fatigue reliability assessment of turbine bladed disks," *International Journal of Mechanical Sciences*, vol. 142-143, pp. 502–517, 2018.

[3] X. Chen, P. Berring, S. H. Madsen, K. Branner, and S. Semenov, "Understanding progressive failure mechanisms of a wind turbine blade trailing edge section through subcomponent tests and nonlinear FE analysis," *Composite Structures*, vol. 214, pp. 422–438, 2019.

[4] E. Kementzetzidis, S. Corciulo, W. G. Versteijlen, and F. Pisanò, "Geotechnical aspects of offshore wind turbine dynamics from 3D non-linear soil-structure simulations," *Soil Dynamics and Earthquake Engineering*, vol. 120, pp. 181–199, 2019.

[5] Y. Tominaga and T. Stathopoulos, "CFD modeling of pollution dispersion in a street canyon: comparison between LES and RANS," *Journal of Wind Engineering & Industrial Aerodynamics*, vol. 99, no. 4, pp. 340–348, 2011.

[6] P. Moonen, V. Dorer, and J. Carmeliet, "Evaluation of the ventilation potential of courtyards and urban street canyons using RANS and LES," *Journal of Wind Engineering & Industrial Aerodynamics*, vol. 99, no. 4, pp. 414–423, 2011.

[7] S. Rhea, M. Bini, M. Fairweather, and W. P. Jones, "RANS modelling and LES of a single-phase, impinging plane jet," *Computers and Chemical Engineering*, vol. 33, no. 8, pp. 1344–1353, 2009.

[8] B. Blocken, "LES over RANS in building simulation for outdoor and indoor applications: a foregone conclusion?," *Building Simulation*, vol. 11, no. 5, pp. 821–870, 2018.

[9] U. Piomelli, "Wall-layer models for large-eddy simulations," *Progress in Aerospace Sciences*, vol. 44, no. 6, pp. 437–446, 2008.

[10] S. Hawendi and S. Gao, "Impact of windward inlet-opening positions on fluctuation characteristics of wind-driven natural cross ventilation in an isolated house using LES," *International Journal of Ventilation*, vol. 17, no. 2, pp. 93–119, 2018.

[11] J. Liu and J. Niu, "CFD simulation of the wind environment around an isolated high-rise building: an evaluation of SRANS, LES and DES models," *Building and Environment*, vol. 96, pp. 91–106, 2016.

[12] A. Elshaer, H. Aboshosha, G. Bitsuamlak, A. El Damatty, and A. Dagnew, "LES evaluation of wind-induced responses for an isolated and a surrounded tall building," *Engineering Structures*, vol. 115, pp. 179–195, 2016.

[13] Z. T. Ai and C. M. Mak, "Large-eddy simulation of flow and dispersion around an isolated building: analysis of influencing factors," *Computers and Fluids*, vol. 118, pp. 89–100, 2015.

[14] N. Y. O. A. M. N. S. Masao, "Wind response of horn-shaped membrane roof and proposal of gust effect factor for membrane structure," *Journal of the International Association for Shell and Spatial Structures*, vol. 53, no. 3, pp. 169–176, 2011.

[15] W. U. Yue, C. H. E. N. Zhao-qing, and S. U. N. Xiao-ying, "Research on the wind-induced aero-elastic response of closed-type saddle-shaped tensioned membrane models," *Journal of Zhejiang University-Science A (Applied Physics & Engineering)*, vol. 16, no. 8, pp. 656–668, 2015.

[16] K. Arjun, S. Xiaoying, and W. Yue, "Wind-induced responses and equivalent static design method of oval-shaped arch-supported membrane structure," *Journal of Wind Engineering & Industrial Aerodynamics*, vol. 213, article 104620, 2021.

[17] P. Mariangela and P. Spinelli, "Dynamic analysis based design of cable structures," *Bulletin of IAss*, vol. 30, pp. 93–107, 1989.

[18] B. Tabarrok and Z. Qin, "Dynamic analysis of tension structures," *Computers & Structures*, vol. 62, no. 3, pp. 467–474, 1997.

[19] H. Kawai, R. Yoshie, R. Wei, and M. Shimura, "Wind-induced response of a large cantilevered roof," *Journal of Wind*

Engineering and Industrial Aerodynamics, vol. 83, no. 1-3, pp. 263–275, 1999.

[20] F. J. Sun, D. M. Zhang, and Z. X. Yin, "Research on wind-induced response of cable-membrane structure considering vertical pulsant wind," *Steel Construction*, vol. 2, pp. 9–13, 2007.

[21] L. X. Li, Y. Q. Xiao, and L. L. Song, "Study on fluctuating wind characteristics of tower A of Hong Kong Zhuhai Macao Bridge Project," in *Proceedings of the 6th national civil engineering graduate academic forum [C]*, p. 1, Education Committee of China Society of Civil Engineering: China Society of Civil Engineering, 2008.